A STEREO-VISION BASED HAZARD-DETECTION ALGORITHM FOR FUTURE PLANETARY LANDERS.

Svenja Woicke[1] **and Erwin Mooij**[2]

[1]*PhD student, Delft University of Technology, Kluyverweg 1 2629HS Delft The Netherlands, s.woicke@tudelft.nl*
[2]*Assitant Professor, Delft University of Technology, Kluyverweg 1 2629HS Delft The Netherlands, e.mooij@tudelft.nl*

ABSTRACT

A great research interest in the field of planetary and lunar landings, is to increase the robustness and autonomy of landing vehicles. One of the possibilities to increase them both is by integrating hazard detection and avoidance into the landing system. Such an algorithm is capable of detecting surface hazards and avoiding these by steering the spacecraft towards a safe landing site. In this paper a hazard detection algorithm is presented. This algorithm can detect surface slope, surface roughness, and illumination. To obtain a final hazard map of the surface, this information is combined into a final hazard map. This is shown for one sample scene. In addition, a sensitivity analysis concerning altitude and baseline is presented. It is concluded that stereo-vision based hazard detection is possible for altitudes of $\leq$ 200 m with baselines of 2 m. Therefore, stereo vision is a feasible algorithm for hazard detection and avoidance for future planetary landers.

Key words: Hazard detection and avoidance, final descent, planetary and Lunar landing.

1. INTRODUCTION

For scientific exploration of the Solar system, landing vehicles are an important tool. However, performing a soft landing on any of these bodies is far from a trivial task. There are plenty of problems to be overcome, one of these is how to detect and avoid surface hazards, when they are present in the landing region.

For the Moon and Mars digital elevation models (DEMs) of sufficient resolution are available to select landing sites, which are inherently safe, i.e., are known to not contain any hazardous slope or roughness prior to landing. However, requiring such inherently safe landing sites will greatly restrict the landing-site selection. Moreover, less smooth terrain is commonly more interesting from a scientific point of view. For the other Solar system bodies, DEMs of sufficient resolution are not available, thus no inherently safe landing sites can be selected.

In case of landing in regions, which are not inherently safe, it is a necessity for the lander to be equipped with a hazard detection and avoidance (HDA) system. It has to be noted that such a system will require an additional, and new capability of the landing system, namely precision landing. Current landing GNC systems would be unable to process the information provided by the HDA system.

In this paper hazard detection (HD), a part of the HDA system, is discussed in more detail. The presented algorithm makes use of a camera-based stereo-vision system. Using a camera-based system was a design choice made based on the low mass, power consumption, volume, and cost of cameras as opposed to active sensors such as radar and LIDAR. LIDAR-based HDA systems are, for example, discussed in [1, 2, 3]. Research on camera-based systems is, e.g., presented in [4, 5]; note that these systems are mono-camera systems rather than stereo-camera systems. Based on the fundamental equations of stereo vision the achievable depth resolution of an elevation map is strongly depending on the baseline and the altitude. Thus, it is very important to determine the limitations of the stereo algorithm concerning these parameters. Therefore, the purpose of this paper is to show, based on a sensitivity analysis, the performance envelope of a stereo-vision based hazard-detection algorithm.

This paper starts by presenting the requirements for this algorithm. This is followed by a brief description of the algorithm in Section 2. In Section 3, the resulting maps for a sample scene are presented and discussed. The sensitivity analysis of the proposed algorithm is covered in Section 4. The paper concludes with some final remarks in Section 5.

2. ALGORITHM REQUIREMENTS

The HD algorithm is supposed to detect hazards. It is necessary to determine which kind of surface features are hazardous to the lander and should therefore be avoided. Hazards are posed by:

- Slope

- Rocks and boulders
- Smaller craters
- Shadow

Rocks, boulders, and smaller craters can be summarised under the category of "roughness" which describes all features that deviate from the local mean-plane.

Based on reference missions such as the ESA Lunar Lander [6], NASA Mars Science Laboratory [7] and reference projects such as NASA ALHAT[1], the following requirements were derived:

1. The algorithm shall be able to detect rocks and boulders, i.e., roughness, > 0.5 m.
2. The algorithm shall be capable of detecting slopes $> 15°$.
3. The algorithm shall be able to lead to $> 99\%$ safe landing-site classifications.
4. The number of un-safesites labelled as safe shall be $\leq 1\%$.
5. The algorithm shall be executable in ≤ 2 s, on a personal computer.

Here, it must be noted that requirement 3 can only be tested if the HD system is integrated in a full guidance, navigation, and control (GNC) system. Using the combination of HDA and GNC, it would then be possible to run landing simulations and determine the number of safe landings over multiple runs. As this papers focuses on the HD system only, requirement 3 is not analysed.

3. ALGORITHM

The algorithm uses stereo-vision techniques for computing the DEM from two input images. The stereo images are obtained using a fixed stereo set-up of known baseline. Disparities are computed using block matching based on the sum-of-squared differences. To obtain sub-pixel disparities, thereby improving the depth resolution, a parabolic fit is used.

From the DEM slope as well as roughness are computed. Slope is computed by fitting a mean plane trough a local window of the DEM. The roughness is defined as the deviation from the local mean plane of each pixel. In addition to DEM-based roughness also texture-based roughness is computed. Here, a histogram-based variance algorithm is used. Lastly, the algorithm can also detect shadows based on image intensity.

The algorithm is based on the algorithm described in [8], with the only addition of sub-pixel disparity estimation by means of a parabolic fit rather than up-sampling. A full description of the current algorithm and the design trade-offs is presented in [9]. Comparing the results presented in [8] to the results presented in Section 4, it is apparent how much the implementation of the parabolic fit increased the quality of the DEMs.

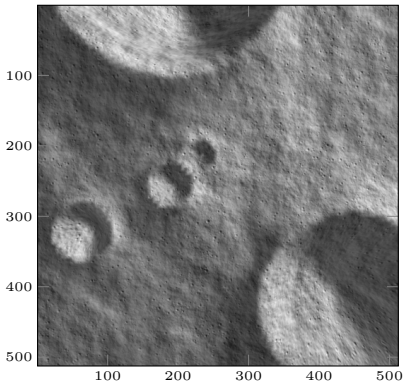

Figure 1. The input scene

4. SAMPLE RESULTS

To demonstrate the working principle of the algorithm and to proof that the algorithm works as desired, the full results for one HD run are given below. The sample results are obtained for a spacecraft at 150 m altitude above the lading region with a fixed baseline of 2 m. The size of the stereo input images is 512×512 px.

The scene, as well as, the stereo images were created using the Planet and Asteroid Natural Scene Generation Utility (PANGU) [10]. Figure 1 shows the input scene imaged at 150 m. The camera's field of view is $30°$. For the stereo-vision algorithm two of these input images are required. Both are taken at the same altitude but with a horizontal off-set of 2 m.

Figures 2a and b show the computed DEM and the ground-truth DEM, respectively. It can be seen that the ground-truth is slightly smoother than the computed DEM, however, all features and changes in elevation are resolved well.

For the slope and the DEM-based roughness, as presented in Figures 3 and 4, respectively, the same conclusions can be drawn: the true maps are slightly smoother, however, the overall result is very good. For the slope and the roughness maps, it has to be noted that the algorithm tends to slightly overestimate larger slopes and roughness. As these have to be avoided anyway, this can be seen as a safety factor.

Figure 5 shows the resulting texture map (texture-based roughness). From the texture-detection algorithm it is expected that it will detect crater rims, rocks and boulders. Comparing the texture map in Figure 5 to the input image

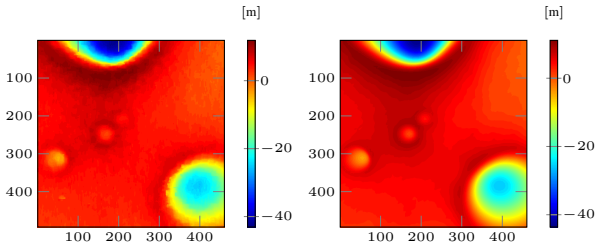

(a) DEM computed (b) DEM true

Figure 2. Ground truth DEM and computed DEM compared.

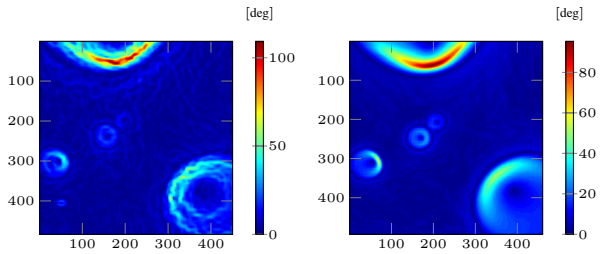

(a) Slope computed (b) Slope true

Figure 3. Ground truth slope and computed slope compared.

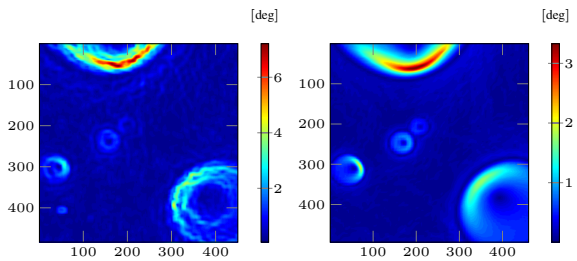

(a) Roughness computed (b) Roughness true

Figure 4. Ground truth roughness and computed roughness compared.

in Figure 1 it can be concluded that the algorithm performs this task successfully, as the rims of all five craters are detected.

Figure 6a shows the final hazard map, after combining slope, roughness and texture information. The red regions, are those that are hazardous based on the requirements specified in Section 2 (slopes $\geq 15°$ and roughness $\geq 0.5\,\mathrm{m}$ pose hazards). A map indicating the correctly and wrongly detected hazards is shown in Figure 6b. Here, red regions indicate undetected hazards (located, e.g., at $\approx (20, 300)$) and green regions indicate false alarms (safe regions which the algorithm detected as hazardous). The red regions are those to be minimised.

Table 1 gives the numerical errors for the hazard detection. FN are the false negative errors, undetected hazards, FP are false alarms, TN are correctly detected hazards and TP are correctly detected safe sites. It can be seen that the number of undetected hazards is clearly below

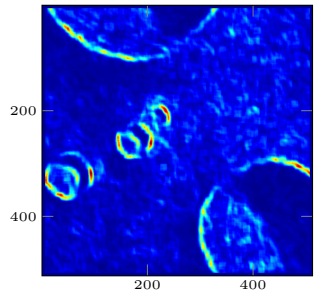

Figure 5. Texture map.

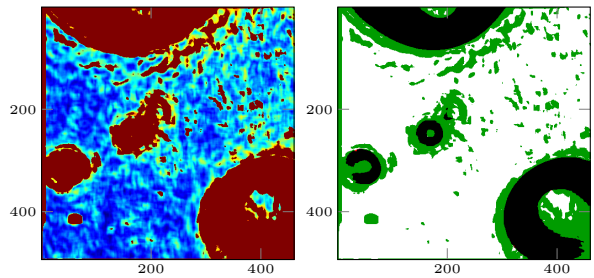

(a) Hazard map (b) Hazard map errors

Figure 6. Hazard map errros and computed hazard map.

1%, as defined in Section 2.

The algorithm took less than 1.5 s to execute for the presented scene. This is less than the required 2 s as stated in Section 2.

5. SENSITIVITY ANALYSIS

As mentioned in Section 1, one of the main issues concerning stereo vision for hazard detection during planetary landings is that its performance will be limited by altitude and baseline. Therefore, it is important to perform a sensitivity analysis to investigate how well the algorithm performs when varying altitude and baseline and therewith determining the limits of the performance envelope.

To this end, two different scenes are used which are imaged at different altitudes using different baselines. Altitudes of 50 m, 75 m, 100 m, 150 m, 200 m, 300 m, and 400 m are tested.

Table 1. Results for the sample scene.

FN	FP	TN	TP	DEM_μ
0.13%	20.10%	15.86%	64.02%	0.47 m
DEM_σ	slp_μ	slp_σ	rgh_μ	rgh_σ
0.39 m	1.98°	2.43°	0.32 m	0.43 m

In Figures 8 to 14 the results of this sensitivity analysis are summarised. Presented are the total number of correct detections per altitude as a function of baseline, the number of undetected hazards (FN), at each tested altitude as a function of baseline, and lastly the DEM mean error as a function of baseline.

The two different scenes, imaged at 400 m altitude are presented in Figure 7. When lower altitudes are tested, the viewing point is lowered towards the center of the images. Clearly, scene 1 is less complex than scene 2 and also contains less slopes. Scene 2 contains multiple craters of different sizes and feature-free regions contain more terrain variation.

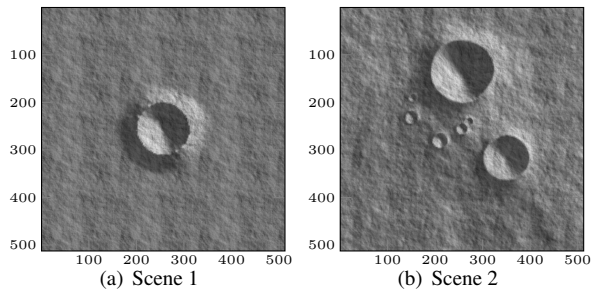

Figure 7. The two scence used for the sensitivity analysis.

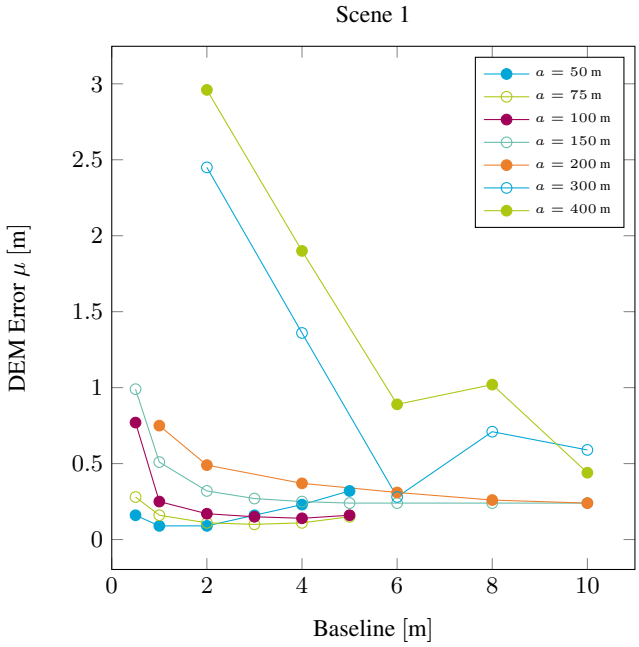

Figure 8. DEM error, μ, as a function of baseline.

5.1. Scene 1

The DEM mean error, μ_{DEM}, is presented in Figure 8. To detect all roughness of 0.5 m purely based on the DEM, obviously, a DEM resolution of $\leq$ 0.25 m would be required. However, since roughness detection is done with a combination of texture and DEM-based detection, less resolution is sufficient, which will be confirmed in Section 5.3. If the requirement for μ_{DEM} is thus relaxed towards accepting all $\mu_{DEM} \leq 0.5$ m, all altitudes of $\leq$ 200 m can deliver sufficient resolutions for baselines $\leq$ 2 m (minimum baseline depending on altitude).

Figure 9 shows the percentage of undetected hazards. The requirement as stated in Section 2 was that not more than 1% is allowable. Investigating Figure 9 it can be concluded that this requirement is met for all baseline and altitude combinations. Because the algorithm is performing so well with respect to undetected hazards, it is important to investigate the number of false alarms (safe sites classified as unsafe) as well. This is done by analysing the number of all correct detections.

The graph showing the number of correct detections for all baseline and altitude combinations is shown in Figure 10. Obviously, too many false alarms are problematic, however, with less than 50% false alarms it should always be possible to select a safe landing site. Thus, it can be concluded that for all altitudes $\leq$ 200 m sufficient correct detections can be archived for baselines of 2 m and even less at the lower altitudes.

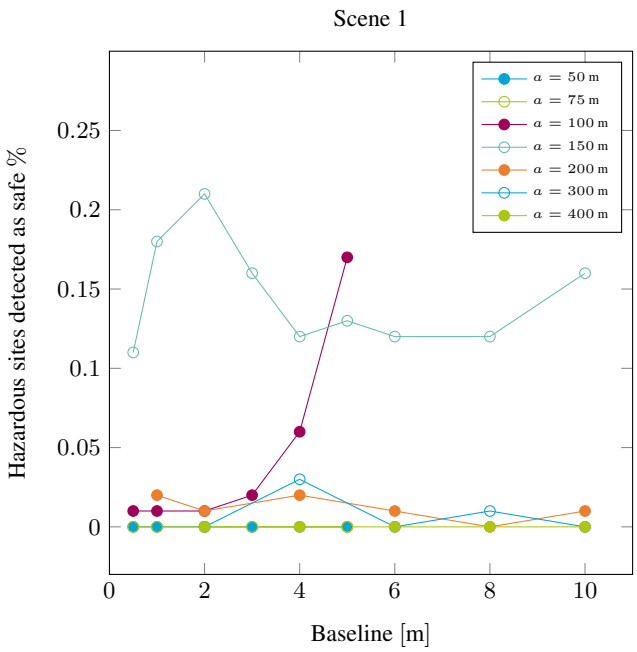

Figure 9. Hazardous site safe detections, FN, as a function of baseline.

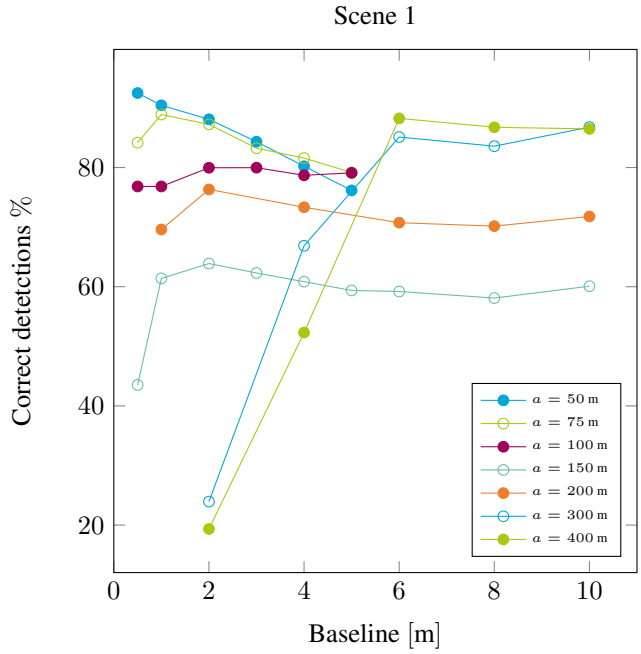

Figure 10. Correct detections, TN+TP, as a function of baseline, Scene 1.

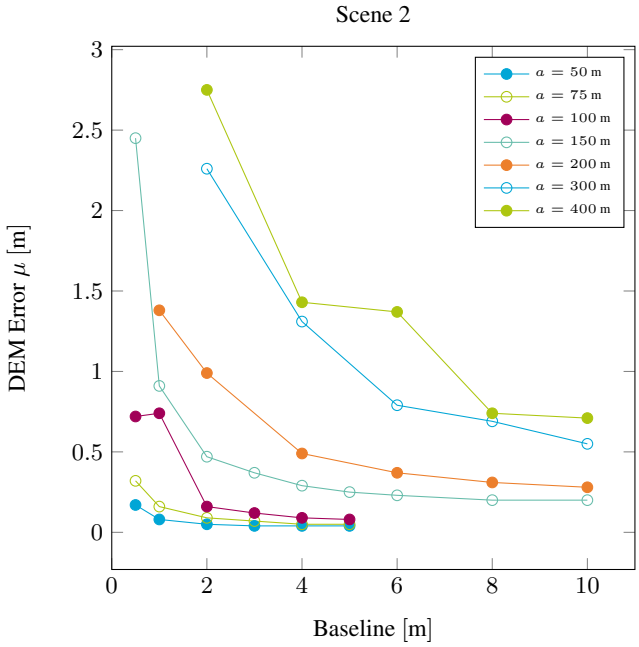

Figure 11. DEM error, μ, as a function of baseline.

5.2. Scene 2

The same graphs as for scene 1 are also created for scene 2. Figure 11 gives the DEM error as a function of altitude and baseline. μ_{DEM} is slightly worse than for the first scene. This is mainly because the complexity of scene 2 is higher and DEM errors mainly occur at locations of extreme terrain change. Still, when investigating Figure 12, it can be seen that, even though μ_{DEM} is higher than for scene 1, the undetected hazards stay below 1% for ≤ 200 m in combination with baselines of ≤ 2 m. Therefore, the slightly higher μ_{DEM} can be accepted.

Figure 13 shows the total number of correct detections. Here, the same conclusions can be drawn as for scene 1. Sufficient correct detections can be archived for altitudes ≤ 200 m with baselines ≤ 2 m.

5.3. Roughness

As mentioned previously, roughness is not detected based on the DEM only, but from a combination of DEM-based and texture-based roughness-detection. Since the requirement for the acceptable DEM error was relaxed assuming that texture detection will assist in detecting hazards smaller than the DEM resolution, this assumption has to be tested. Therefore, multiple rocky scenes were created and imaged at various altitudes. Rocks are counted in the input image as well as in the output maps of DEM-based roughness and texture detection. Figure 14 shows the result. It can be concluded that texture detection always detects all rocks, however, it is unable to

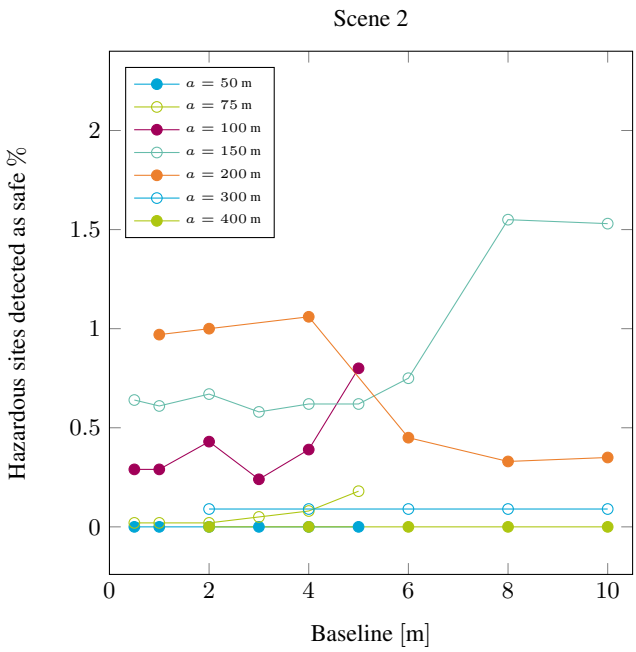

Figure 12. Hazardous site safe detections, FN, as a function of baseline.

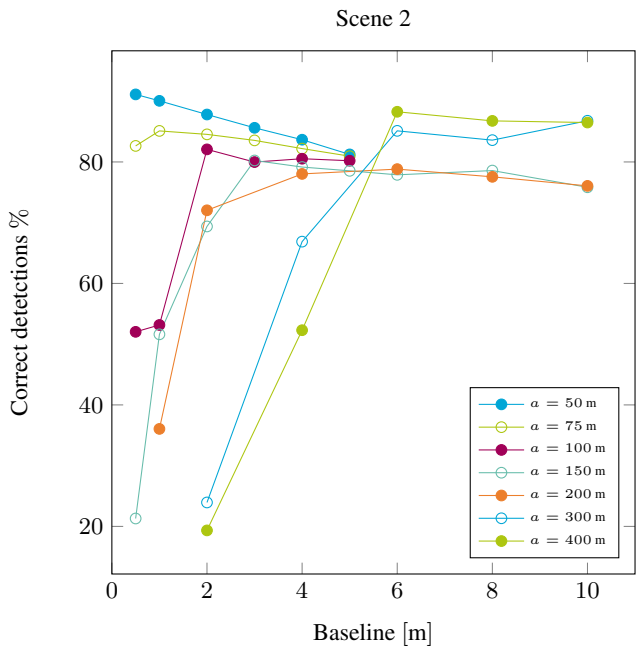

Figure 13. Correct detections, TN+TP, as a function of baseline, Scene 2.

estimate the size of the roughness features. The result of DEM-based roughness is less constant, however, it usually detects at least half of the present rocks. Still, DEM-based roughness has one benefit: it can estimate the size of the roughness features. Two conclusion can be drawn from this: first, the assumption that DEM errors of more than 0.25 m are allowable while still being able to detect all rocks of $\geq$ 0.5 m based on texture detection, was valid. Second, texture detection should be used alongside DEM-based roughness, as both have their own benefits.

For all algorithm executions performed for this sensitivity analysis, the execution time never exceeded 2 s. 2 s were specified as the maximum allowable time in Section 2. Therefore, it can be concluded that the algorithm is sufficiently fast for real-time applications.

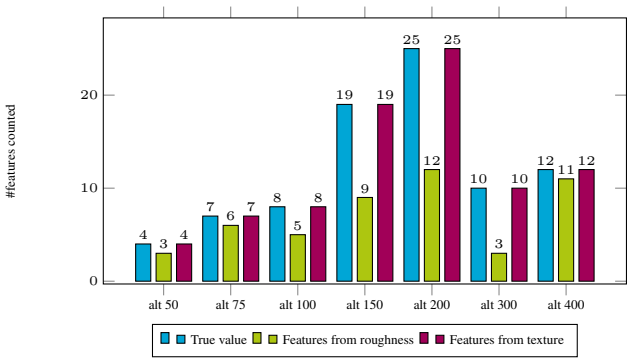

Figure 14. Feature counts at different altitudes.

6. CONCLUSIONS

The developed stereo-vision algorithm proved to be working at altitudes of $\leq$ 200 m. For these altitudes baselines of 2 m, and even less at lower altitudes, are feasible. This magnitude is achievable on current lander designs. If lower altitudes are chosen for mapping, even lower baselines are possible. Moreover, it was shown that stereo vision may be a suitable approach to solve the hazard-detection problem. Also it was shown that combining both texture-based and DEM-based roughness-detection for HD will deliver the most optimal results.

Within the specified performance envelope, the algorithm will never result in more than 1% undetected hazard. Furthermore, it can always be executed within less than 2 s. From the results it can be concluded that the algorithm is a very good candidate HD algorithm for future lander missions.

ACKNOWLEDGEMENTS

We would like to express our gratitude towards the Space Technology Centre of the University of Dundee for providing us with a licence for PANGU.

REFERENCES

[1] C. D. Epp and T. B. Smith. "Autonomous precision landing and hazard detection and avoidance technology (ALHAT)". In: *IEEE Aerospace Conference*. IEEE. 2007, pp. 1–7.

[2] J. de Lafontaine et al. "LAPS: the development of a scanning lidar system with GNC for autonomous hazard avoidance and precision landing". In: *Defense and Security*. International Society for Optics and Photonics. 2004, pp. 81–93.

[3] A. E. Johnson et al. "LIDAR-based hazard avoidance for safe landing on Mars". In: *Journal of guidance, control, and dynamics* 25.6 (2002), pp. 1091–1099.

[4] F. Câmara et al. "Hazard avoidance techniques for vision based landing". In: *6th International ESA Conference on Guidance, Navigation and Control Systems*. 2005.

[5] Y. Cheng et al. "Passive imaging based hazard avoidance for spacecraft safe landing". In: *6th International Symposium on Artificial Intelligence and Robotics & Automation in Space* (2001).

[6] J. D. Carpenter et al. "Scientific Preparations for Lunar Exploration with the European Lunar Lander". In: *Planetary and Space Science* (2012).

[7] D. W. Way et al. “Mars Science Laboratory: Entry, descent, and landing system performance”. In: *IEEE Aerospace Conference*. IEEE. 2007, pp. 1–19.

[8] S. Woicke and E. Mooij. “Stereo-Vision Algorithm for Hazard Detection during Planetary Landings”. In: *AIAA Guidance, Naviagtion and Control Conference, National Harbour, Maryland*. 2014.

[9] S. Woicke and E. Mooij. “A Stereo-Vision Hazard-Detection Algorithm to Increase Planetary Lander Autonomy”. In: (Manuscribt submitted for publication).

[10] S Parkes et al. “Testing advanced navigation systems for planetary landers and rovers”. In: *International Astronautical Congress, Paper IAC-09-A3*. Vol. 1. 2009, p. 69.